ACS APPLIED MATERIALS & INTERFACES

Research Article

www.acsami.org

Dispersion Morphology and Correlation to Moduli Using Buckling Metrology in Clay–Biopolymer Nanocomposite Thin Films

Hongyi Yuan,[†] Gurpreet Singh,[†,∥] Dharmaraj Raghavan,[‡] Abdullah M. Al-Enizi,[§] Ahmed Elzatahry,[§,⊥] and Alamgir Karim*[,†]

[†]Department of Polymer Engineering, The University of Akron, Akron, Ohio 44325, United States

[‡]Department of Chemistry, Howard University, Washington, DC 20059, United States

[§]Chemistry Department, Faculty of Science, King Saud University, PO Box 2455, Riyadh 11451, Saudi Arabia

ABSTRACT: Structure–interaction–mechanical property correlation in bionanocomposite thin films is an area of growing interest for research and application areas from barrier to molecular transport to UV blocking layers for polymer solar cells to dielectric properties modification. Here we study flow coated ultrathin to thin films (70–150 nm) of clay bionanocomposites to understand the nanoparticle dispersion and its effect on nanomechanical properties. Binary and ternary thin film systems of polylactide (PLA), polycaprolactone (PCL), and Cloisite 30B (C30B) clay platelets were investigated. While C30B was only partially intercalated by PLA, it was almost completely intercalated by PCL due to strong hydrogen bonding. In addition, the dispersion of C30B improved continuously and linearly with increasing PCL content in homogeneously cast blended PLA:PCL. GIWAXS confirmed that the intercalated clay platelets in PLA and PCL were dominantly oriented parallel to the substrate. The method of strain induced elastic buckling instability for mechanical measurements (SIEBIMM) showed that pure PLA and PCL had in-plane modulus unchanged from bulk values for this range of ultrathin–thin films. In PLA/C30B nanocomposite thin films, the in-plane elastic modulus rapidly increased by up to 26% with 2 wt % C30B, but saturated thereafter up to 10 wt % C30B forming C30B aggregates. On the other hand, the in-plane elastic modulus of PCL/C30B thin films increased linearly by up to 43% with 10 wt % C30B due to the higher interaction driven dispersion, results that were shown to fit well with the Halpin–Tsai model. We conclude that the different strengthening behavior came from different interaction driven dispersion states of C30B in polymer matrices, governed by their molecular structures.

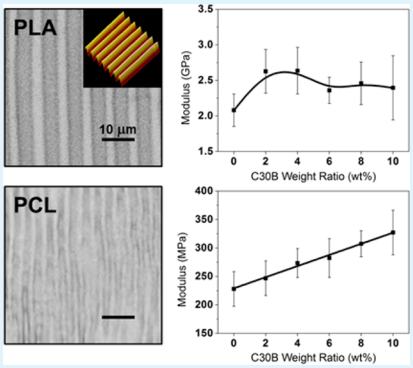

KEYWORDS: *nanocomposite thin films, clay, biopolymer, elastic modulus, state of dispersion*

INTRODUCTION

Biopolymers represent an environment-friendly class of materials, which come from natural sources and provide biocompatibility and biodegradability. Extensive research has been conducted on biopolymers including their synthesis, properties, and applications.[1−4] In order to achieve tunable physical properties (mechanical, thermal, barrier, dielectric, etc.) and expand applications of biopolymers, biopolymer based nanocomposites, or bionanocomposites, have been developed and investigated in great detail.[5−8] Among these, clay biopolymer nanocomposite is one of the most commonly studied systems, which has promising applications including controlled permeation films.[9] The permeates have to travel around the dispersed nanoclays while traversing these thin films, which increases the tortuosity and improves the barrier properties of materials. In order to promote clay dispersion in polymer matrices, organically modified clays or organoclays are commonly used, providing strong interaction between polymers and nanoparticles which facilitates formation of intercalated and/or exfoliated morphologies.

The tortuosity of pathway for permeates to percolate through a nanocomposite thin film is a function of several attributes. Perhaps the most important is the nanofiller anisotropy. If the nanofiller is highly anisotropic in two dimensions, it can be expected to provide the most tortuous pathway based on dimensionality alone. Clay particles in their well-dispersed states are two-dimensional platelets that satisfy this criterion very well. Another important factor is the orientation of the dispersed clay. Clay platelets lying parallel to the film surface would be most effective in enhancing the tortuosity. In addition, the concentration of clay particles in the film is important since an interdigitated overlap of the anisotropic clay platelets is highly desirable. In this paper, we examine all of the above important aspects in bionanocomposite thin and ultrathin films (70–150 nm) at both the molecular and macroscopic level using several advanced characterization methods.

Received: December 7, 2013
Accepted: July 25, 2014
Published: July 25, 2014

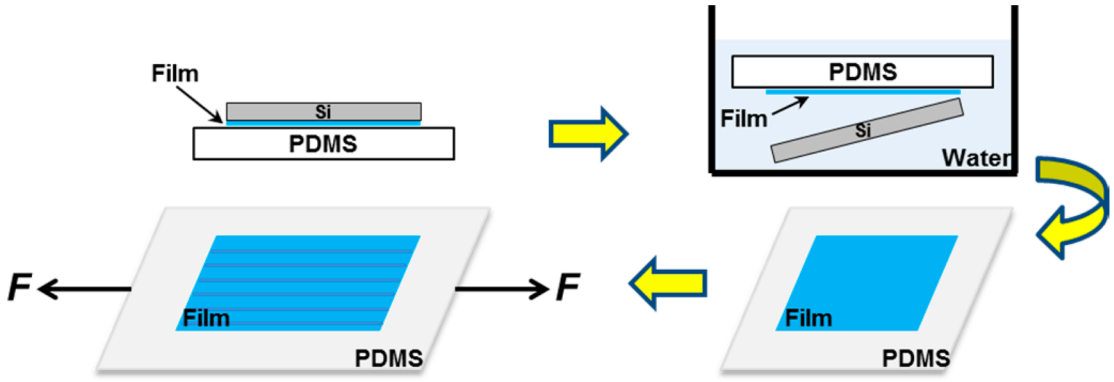

Figure 1. Schematic of SIEBIMM procedures.

In addition to barrier properties, mechanical properties of thin films become important as these films are subject to various forms of mechanical stresses and deformations including flexing, stretching, and wrinkling. For potential gas membrane applications of these films, there can be significant pressure of gases that needs to be supported without rupture. In fact, polymer films as thin as 18 nm have recently been investigated for gas permeability.[10] In these regards, many polymeric materials cannot be used as freestanding thin films due to their limited dimensions affecting the mechanical durability but nevertheless have the potential for applications as surface layers on coatings and permeation films. It is therefore crucial to characterize the elastic modulus of these thin films and understand if it can be enhanced by adding nanoparticles, as it determines the scope of their applications. Unfortunately, conventional methods for modulus measurements, such as tensile test or nanoindentation, are not suitable for thin films due to reasons of geometric limitations and instrumental sensitivity.

In the past decade, a novel technique known as strain-induced elastic buckling instability for mechanical measurements (SIEBIMM) was developed for mechanical characterization of submicron thin films.[11] The theoretical background is the buckling instability that occurs in a system composed of a stiff, thin film and a soft, thick substrate.[12] When a compressive stress is applied to the system, the surface must buckle in order to accommodate for the large difference in moduli of the film and the substrate, which generates a periodic buckling pattern. The wavelength of the buckling pattern is related to modulus of film, modulus of substrate, Poisson's ratios and film thickness by the following equation:

$$\frac{E_f}{(1-\nu_f^2)} = \frac{3E_s}{(1-\nu_s^2)}\left(\frac{d}{2\pi h}\right)^3$$

where E and ν are the modulus and Poisson's ratio, respectively. Subscript f stands for film and s for substrate. d is the buckling wavelength and h is the film thickness. E_f can be calculated if other parameters are known or directly measurable.

SIEBIMM proves to be an elegant and efficient method that yields the elastic moduli of thin films in a rapid and accurate manner. It has been applied to various polymer systems such as polyelectrolyte multilayers,[13,14] polymer brushes,[15] soft polymer networks,[16] and block copolymers.[17] In one example, SIEBIMM has also been carried out to measure elastic moduli of PS/CdSe nanocomposite thin films.[18] In this paper, we apply the SIEBIMM method to clay-biopolymer nanocomposite thin films for the first time.

Polylactide and polycaprolactone were used as the polymer matrices as they have promising biomedical and packaging applications and are extensively studied in the bulk form. Cloisite 30B was chosen as the nanoclay due to its frequent use in biopolymer matrices to prepare bulk nanocomposites, which make good comparison with our present study in thin film nanocomposites. Previously, the dispersion states and strengthening effects of nanoclays, including C30B, have been investigated extensively in both PLA- and PCL-based nanocomposites in their bulk forms.[19−24] However, there is insufficient knowledge on the behavior of nanocomposite submicron thin films, an area where only a handful of papers are reported on nonbiopolymeric systems. For instance, when the lateral dimensions of the clay platelets exceed the film thickness dimensions, can we expect parallel alignment of the clay platelets, and how does this contribute to the elastic modulus? How do we anticipate clay−polymer interactions to control their thin film dispersion states? Given the confined geometries and the specific processing method, the dispersion states of clay in thin films can be significantly different from those in bulk materials. By studying the structure, morphology and elastic modulus, we aim to provide a fundamental understanding of the dispersion and strengthening mechanism in thin films of clay-biopolymer nanocomposites.

EXPERIMENTAL SECTION

Materials and Solutions. Poly(D,L-lactide) (PLA) with weight-average molecular weight M_w = 96000 g/mol was obtained from DURECT Corporation. Polycaprolactone (PCL) with number-average molecular weight M_n = 80000 g/mol was obtained from Sigma-Aldrich. Cloisite 30B (C30B) was obtained from Southern Clay Products. All materials were used as received without further purification. PLA and PCL were dissolved in laboratory grade toluene (BDH Chemicals) to make 2 wt % homopolymer and blend solutions. Different weight fractions of C30B (2, 4, 6, 8, and 10 wt % with respect to the polymer) were subsequently added to the homopolymer or blend solutions, respectively, and then ultrasonicated in a water bath for 2 h using a B2500A-MTH Ultrasonics Cleaner (VWR) to facilitate C30B dispersion.

Si (100) wafers (Silicon Quest International) were used as casting substrates for thin films. Prior to experiments, Si wafers were cleaned by methanol and deionized (DI) water and exposed in a PSD Series Digital UV Ozone System (Novascan) for 30 min to render their surfaces hydrophilic.

Polydimethylsiloxane (PDMS) (Sylgard 182, Dow Corning) was used as the elastomeric substrate for SIEBIMM. The weight ratio of base to cross-linking agent was 19:1. The mixture was hand-stirred for 10 min and cast onto a flat glass substrate. It was then placed in a vacuum chamber for 30 min at room temperature to remove trapped

air bubbles and subsequently heated at 120 °C for 2 h to facilitate cross-linking. The cross-linked PDMS was peeled off the glass substrate and cut into 75 mm × 25 mm × 1 mm strips. The elastic modulus of each strip was measured by a TA.XT Plus Texture Analyzer (Texture Technologies) before use.

Preparation of Thin Films. Homopolymer and nanocomposite thin films with thickness gradients were prepared by flow-coating. Detailed description of flow-coating can be found in the literature.[25] Specifically in this study, the gap between the glass blade and the Si substrate was fixed at 127 μm, with 25 μL of solution used to make each film. Velocities of the blade were controlled in a step manner at 10, 15, 20, 25, and 30 mm/s in order to obtain 5 distinct regions of uniform thickness for each film, while keeping the overall thickness range in 70−150 nm. After flow-coating, films were placed in a vacuum chamber at room temperature for 30 min to remove any residual solvent.

Strain-Induced Elastic Buckling Instability for Mechanical Measurements (SIEBIMM). A F20−UV Interferometer (Filmetrics) was used to measure the thicknesses of 5 random locations on each uniform region of each film. The thickness of each region was taken as the arithmetic mean. PDMS strips were attached to a customized strain stage and kept horizontal and unstrained. Homopolymer and nanocomposite thin films were transferred from Si substrates to PDMS using a water-wetting technique.[26] A schematic of procedures is given in Figure 1. Specifically, the film on Si was placed facing down on top of PDMS with the thickness gradient of film (not shown in the schematic for clarity) aligned in the same direction as the length of the PDMS strip, forming a sandwich structure of Si-film-PDMS. After the film completely adhered to the PDMS, the assembly was turned upside down and immersed in DI water, which gradually wetted polymer/Si interface and transferred the film to PDMS. The assembly was taken out of DI water and dried under vacuum for 30 min. The PDMS strip with film was then strained by up to 3% in the length direction, thus applying a compressive stress to the film in the width direction due to the Poisson effect and generating buckling patterns. The wavelengths of buckling patterns were calculated using image processing software ImageJ (National Institutes of Health). A fast Fourier transform (FFT) was performed on each optical image. The distance between first order peaks of the FFT image was measured and converted to the buckling wavelength.

Thin Film Characterization. Morphology of homopolymer and nanocomposite thin films was examined using an Olympus BX41 optical microscope and a DI-Veeco Nanoscope V atomic force microscope (AFM). Dispersion of C30B in polymer matrices was observed by a JEM 1200XII transmission electron microscope (TEM). Wide-angle X-ray scattering (WAXS) was taken using a D8 Discover X-ray diffractometer (Bruker) with a Cu Kα (λ = 0.15418 nm) X-ray source. Grazing-incidence wide-angle X-ray scattering (GIWAXS) measurements were performed at the X9 beamline of the National Synchrotron Light Source at Brookhaven National Laboratory using an incident X-ray beam of energy 13.5 keV (λ = 0.0918 nm). X-ray photoelectron spectroscopy (XPS) survey scans were obtained using a PHI 5000 VersaProbe II Scanning XPS Microprobe with a monochromatic Al Kα source (1486.6 eV) operating at 25 W. Water contact angles were measured at room temperature by a Ramé-Hart model 500 Advanced goniometer with Dropimage Advanced V2.4 software. Differential scanning calorimetry (DSC) measurements were carried out using a Q200 Differential Scanning Calorimeter (TA Instruments). Samples were first heated at high temperatures (200 °C for PLA system and 120 °C for PCL system) for 2 min in order to erase their thermal history, followed by cooling to −90 °C and second heating at the rate of 10 °C/min. Data analysis was completed using Universal Analysis 2000 software (TA Instruments).

RESULTS

Homopolymer and nanocomposite thin film samples were prepared by flow-coating, which is a high-throughput technique and is adaptable to combinatorial methods and roll-to-roll production. In general, by varying experimental parameters, samples with property gradients (thickness, concentration, etc.) and processing gradients (temperature, UV exposure, etc.) can be prepared. Previously, researchers used gradient samples and combinatorial methods to investigate structure and morphology of polymer thin films, which greatly improved the resolution and reliability.[27−30] In this study, the blade velocity of flow-coating was varied in a step-incremental manner, generating thin film samples with step-thickness gradient. Figure 2 shows a

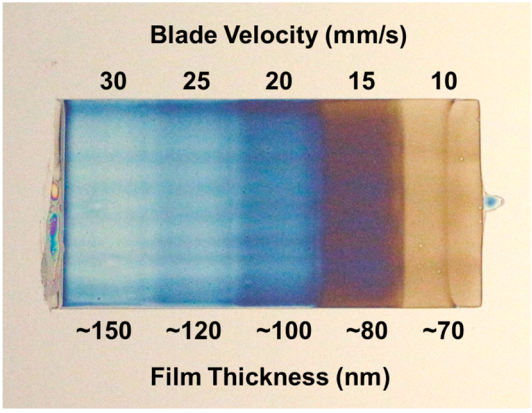

Figure 2. PLA thin film sample with thickness gradient prepared by flow coating.

PLA thin film sample prepared this way with five thickness regions clearly indicated by five different colors due to interference of light at the film surface and the film−substrate interface. Since multiple data points can be collected from one sample, it serves as a high throughput technique which greatly improves not only the efficiency but also the comparative accuracy of experiments.

We first characterized dispersion of C30B in PLA and PCL using WAXS, since nanoparticle dispersion influences the properties and applications of polymer nanocomposites. C30B is a natural montmorillonite organo-modified with a quaternary ammonium salt, which is commonly used as an additive for plastics to improve their physical properties. The organic modifier in C30B is MT2EtOH (methyl, tallow, bis-2-hydroxyethyl, quaternary ammonium). C30B has a disk shape and a layered structure, with each disk around 1 nm thick and 70−150 nm in diameter. The interlayer distance between neighboring disks is 1.8 nm according to manufacturer's documentation (Southern Clay Products). This distance is confirmed by its WAXS spectrum as shown in Figure 3a. The characteristic peak of C30B at 4.95° (location 1) is clearly observed, which corresponds to a distance of 1.8 nm as calculated by Bragg's law.

In PLA/C30B nanocomposite systems, the characteristic peak of C30B is still visible (Figure 3b, location 1). In addition, another peak is observed at a lower angle (~2.60°, location 2) for each weight ratio of C30B. The position of this peak corresponds to a scattering distance of 3.4 nm, which is increased from 1.8 nm by 90%, meaning that the interlayer distance of C30B was expanded by intercalation of PLA molecules. The expansion can be explained by hydrogen bonding between carbonyl groups in the polymer matrix and hydroxyl groups in the quaternary ammonium functionalized organoclay, as found by previous studies.[31] Coexistence of peaks 1 and 2 suggests that some C30B layers were intercalated by PLA while others maintained their original structure in the

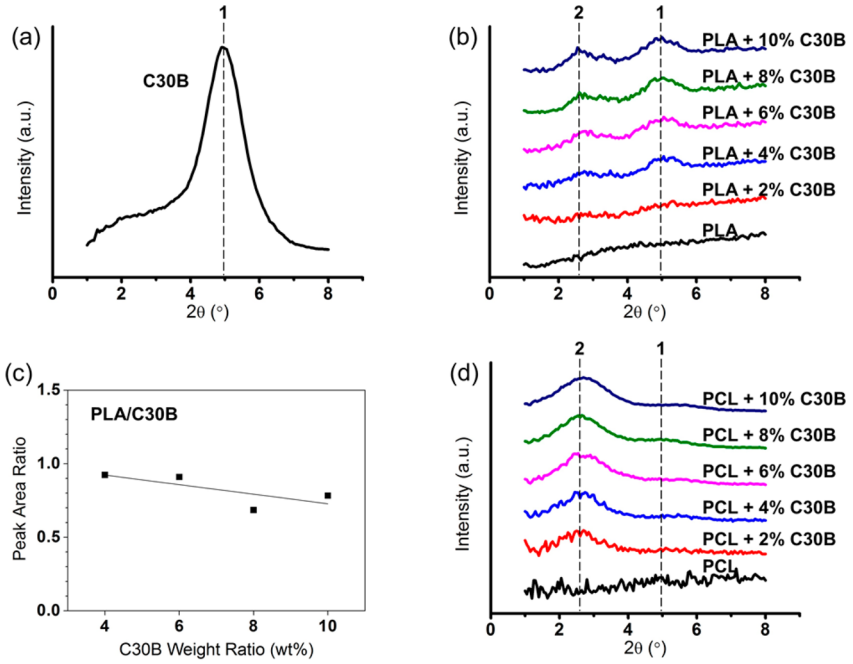

Figure 3. (a) WAXS spectrum of C30B; (b) WAXS spectra of PLA/C30B system; (c) peak area ratios between peaks 2 and 1 in PLA/C30B system; and (d) WAXS spectra of PCL/C30B system. Peaks 1 are characteristic peaks of C30B and peaks 2 correspond to intercalated gallery spacing of C30B.

composite. Figure 3c shows the area ratio between peak 2 and peak 1 for each PLA/C30B nanocomposite (except for PLA +2% C30B as its peaks can be hardly defined), which gives a direct comparison between the amount of intercalated and original C30B nanoparticles. The area ratio decreases roughly linearly with C30B in a small range from 0.9 to 0.7, which corresponds to 48% ∼ 41% intercalation of C30B. Therefore, the dispersion of C30B in PLA is moderate.

An entirely different dispersion state of C30B is found in PCL systems, as shown in Figure 3d. The characteristic peak of C30B (location 1) is absent in PCL/C30B nanocomposites from 2 to 6 wt %, and only barely noticeable for 8 and 10 wt % weight ratios. Instead, a strong peak (location 2) is observed at ∼2.50° for all weight ratios, corresponding to an expanded interlayer distance of 3.5 nm, increased from 1.8 nm by 94%. This suggests that most C30B platelets were largely intercalated by PCL, up to 10 wt % loading which is substantial. In other words, PCL/C30B formed almost completely intercalated nanocomposites and the dispersion of C30B in PCL was fairly uniform. Similar to PLA/C30B, intercalation came from hydrogen bonding by carbonyl groups in the polymer and hydroxyl groups in the nanoclay, and the interlayer distance of C30B was expanded almost identically by both polymers. The difference arises from the chemical structure difference between PLA and PCL as discussed later.

We further confirmed the structure of PLA/C30B and PCL/C30B and studied the orientation of C30B layers in corresponding thin films using grazing incidence wide-angle X-ray scattering (GIWAXS). The X-ray incidence angle was chosen both below the critical angle (α_c) of the film, in which case only the surface is surveyed, and above α_c so that the whole film is examined. Figure 4 shows GIWAXS images on both polymer +10 wt % C30B thin films with incidence angles below and above α_c, as well as their corresponding line profiles along the z- and *y*-directions. The intercalation peak of C30B is observed in each case as shown in Figure 4a−d. The characteristic peak of C30B is clearly noticed in PLA + 10 wt % C30B at q_z = 0.35 Å^{-1}, but the intensity is much weaker in PCL + 10 wt % C30B, which can be more obviously seen in Figure 4e. This observation agrees with previous WAXS results, confirming partial intercalation in PLA/C30B and almost complete intercalation in PCL/C30B.

More importantly, all peaks are found to have much higher intensities in the out-of-plane direction (z) compared with the in-plane direction (y), as shown by the line profiles in *z*- and *y*-directions in Figure 4e and (f), respectively. The intensity scale is the same for a given sample so that intensities along *z*- and *y*-directions can be directly compared. This anisotropy in scattering intensity is a direct reflection of the anisotropic distribution of C30B platelets oriented parallel to the substrate versus perpendicular to the substrate. Peak positions in *z*-profiles match their positions in WAXS for the same C30B concentration. There is virtually no peak in *y*-profiles except for shoulders near the beam stop. This observation indicates that the intercalated C30B layers are mostly stacked along the *z*-direction for both PLA/C30B and PCL/C30B thin films. In other words, they are aligned parallel to the substrate. This parallel orientation is expected, as C30B platelets have a high aspect ratio (∼110), making it difficult or nearly impossible to stand perpendicular to the substrate in these thin films. This is advantageous, since the parallel orientation of C30B is favored for barrier properties wherein the permeates would have to traverse a more tortuous pathway around the nanoparticles before they can reach the other side of the film.

The relative dispersion states of C30B in PLA and PCL were also revealed by TEM, as shown in Figure 5. As seen in Figure 5a,b, C30B are nonuniformly distributed in PLA matrix, with a moderate extent of intercalation and occasional tactoid structures. In contrast, Figure 5c,d show uniform distribution of C30B in the PCL matrix. Most C30B layers were intercalated by the PCL polymer. The trend in TEM results in different

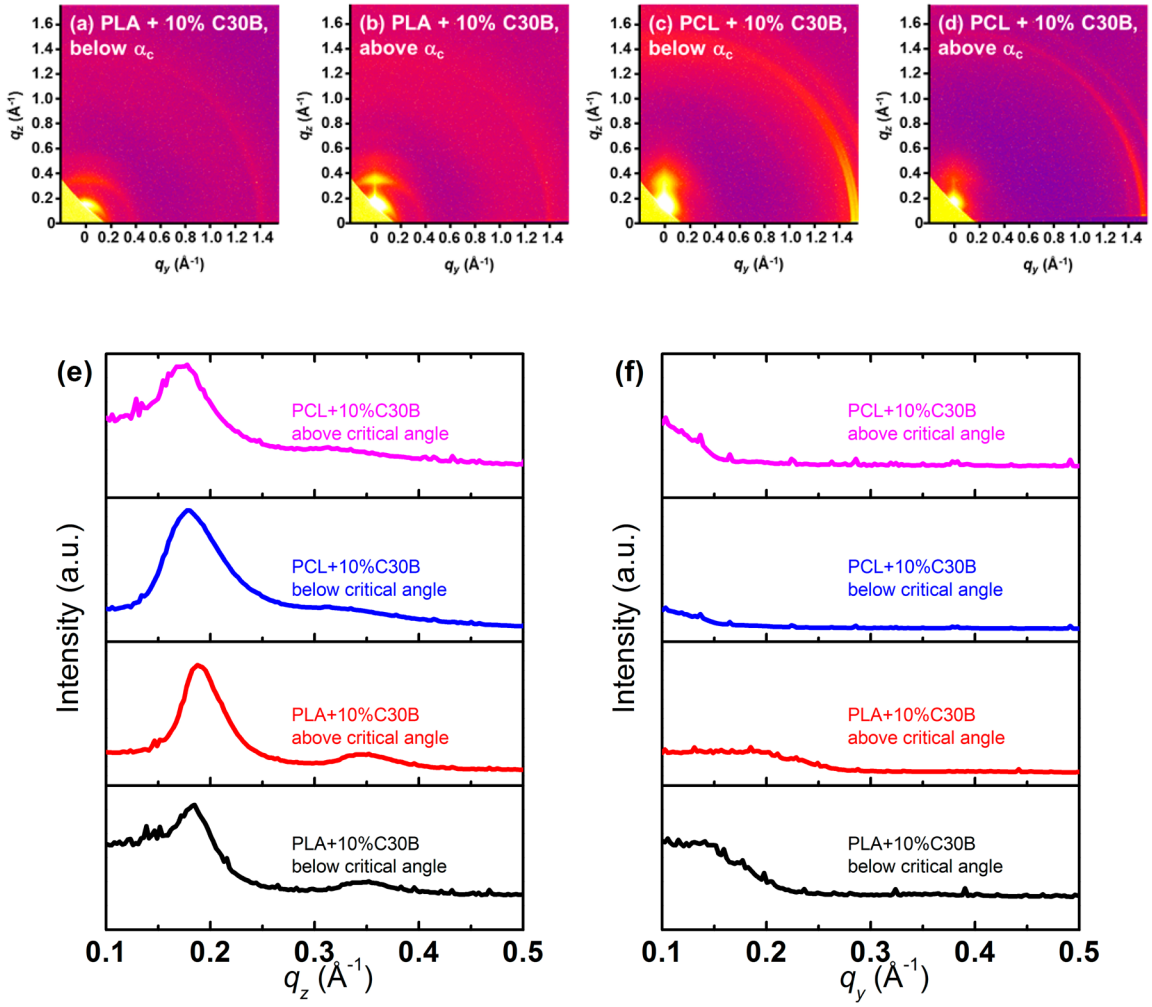

Figure 4. GIWAXS images of nanocomposite thin films: (a) PLA+10%C30B, below α_c; (b) PLA+10%C30B, above α_c; (c) PCL+10%C30B, below α_c; (d) PCL+10%C30B, above α_c. Corresponding line profiles along *z*- and *y*-directions are shown in (e) and (f), respectively.

polymer matrices is in good agreement with results by WAXS and GIWAXS.

The surface properties of nanocomposite thin films can reveal important information about layering of nanoparticles near surfaces, and were investigated by X-ray photoelectron spectroscopy (XPS) and water contact angle measurements. Figure 6 gives the spectra of XPS survey scans on PLA/C30B and PCL/C30B nanocomposites. The Si 2s and 2p peaks are clearly shown in both systems, which could only originate from C30B. As XPS is only sensitive to the top 5−10 nm of the surface material, these peaks confirm the existence of C30B on the surface of nanocomposite thin films. Interestingly, the relative intensities of Si peaks from C30B are independent of the overall weight fraction of C30B in the nanocomposite for both PCL and PLA systems. More importantly, the surface atomic percentages of Si calculated from XPS spectra for all samples were in the order of 10 at%, significantly higher than the overall atomic percentages of Si in nanocomposite thin films (0.1−1 at%) calculated from their weight fractions. XPS only probes the top 2−3 nm of the top film surface, so this signal must arise from the clay platelets present at the film surface. We therefore conclude that not only are the C30B platelets stacked parallel to the substrate within the film, they also form a significantly segregated layer at the film surface within the top 10 nm. Such a surface layering of C30B can be beneficial to the gas barrier properties of nanocomposite thin films, acting as a top-layer barrier coating while also enhancing the nanomechanical properties such as scratch resistance. Future studies will aim to engineer this aspect of surface segregated clay platelets such as its layer thickness with temperature and film thickness.

As a confirmation of XPS determined C30B segregation at the film−air interface, we measured the contact angles of bionanocomposite thin films. Figure 7 shows the effect of C30B on the water contact angles of nanocomposite thin films at room temperature. As neat PLA and C30B have very similar contact angles of 86° and 88°, respectively, there is only a small change in contact angle in PLA/C30B nanocomposites. On the other hand, neat PCL has a lower contact angle of 80°. Notably, adding C30B increases the contact angle of PCL/C30B nanocomposites to the range of 84° ∼ 87° indicating partial surface distribution of C30B. The water contact angles of the nanocomposite thin films are relatively independent of clay concentration in the film, similar to what is obtained from the XPS results.

As blending polymers can typically combine the advantageous properties of the components, we also examined the role of clay addition to blended mixtures of PLA and PCL over a systematic range from the previously studied pure PLA to pure PCL. PLA and PCL were mixed homogeneously in toluene and

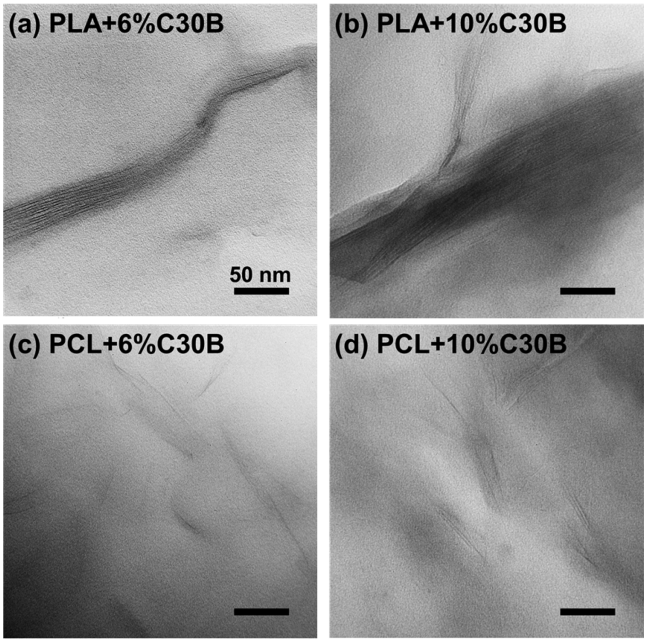

Figure 5. TEM images of (a) PLA+6% C30B, (b) PLA+10% C30B, (c) PCL+6% C30B, and (d) PCL+10% C30B. Scale bars represent 50 nm.

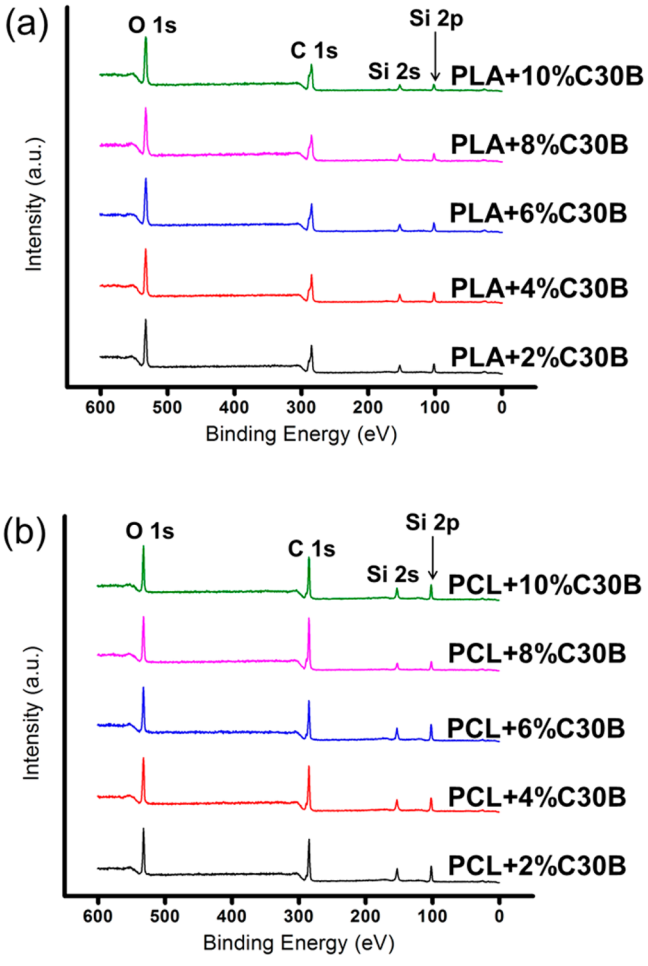

Figure 6. XPS spectra of (a) PLA/C30B system and (b) PCL/C30B system. The Si 2s and 2p peaks originate from C30B.

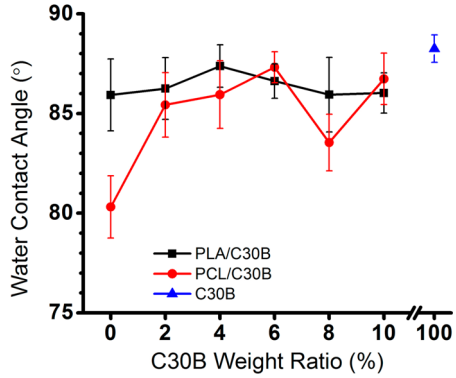

Figure 7. Water contact angles of PLA/C30B system, PCL/C30B system and pure C30B. The values for both systems are slightly below that of pure C30B and relatively independent of C30B concentration, indicating partial enrichment of C30B at the film surface.

cast to form blend films. To maintain the homogenized structures, all films were prepared as cast without thermal annealing. Three concentrations of as-cast blends were chosen, namely 75PLA/25PCL, 50PLA/50PCL, and 25PLA/75PCL, numbers indicating weight percentage of components. C30B was added to each blend for the same weight ratios as in the previous homopolymer films (from 0 to 10 wt % with respect to polymers, respectively). The WAXS spectra of these systems and the corresponding peak area ratios of PLA:PCL + 10 wt % C30B are shown in Figure 8.

Comparing Figure 8a–c, the dispersion of C30B improves as the weight percentage of PCL increases as indicated by weaker characteristic peaks of C30B (location 1) and stronger polymer intercalation peaks (location 2). These results are consistent with the fact that the blend films were quenched into a homogeneous state, which leads to a smooth transition from C30B dispersion in pure PLA to that in pure PCL. The behavior is clearly seen in Figure 8d. As the concentration of PCL in blends increases, the area ratio between the intercalation peak and the original peak of C30B increases roughly linearly from 0.8 (pure PLA) to 4.4 (25PLA75PCL), indicating continuously improved dispersion of C30B.

Finally, the nanomechanical properties via measurements of the elastic moduli of these nanocomposite thin films were investigated using the method of strain induced elastic buckling instability for mechanical measurements (SIEBIMM). According to the SIEBIMM model, buckling occurs when a thin, stiff film is adherent to a thick, soft substrate and the system experiences a compressive stress. This is precisely the case for PLA/C30B and PCL/C30B thin films transferred to elastomeric PDMS substrates and stretched. After stretching, periodic buckling patterns are observed in all homopolymer and nanocomposite thin films as shown in Figure 9. The AFM height image of buckling patterns in neat PLA is given as the inset of Figure 9a showing high fidelity periodicity. Due to this periodicity, the buckling wavelength can be measured directly from the optical or AFM images in real space, which is about 7.3 μm for this sample. Good agreement is found when comparing the values obtained in real space and by FFT (i.e., in reciprocal space), with discrepancies smaller than 2%. All buckling wavelengths in this study are calculated using FFT analysis since it averages over the entire image. In addition, the buckling amplitude can also be found from the AFM height image, and measured to be around 600 nm in this case. It has been shown that the amplitude is also related to the elastic

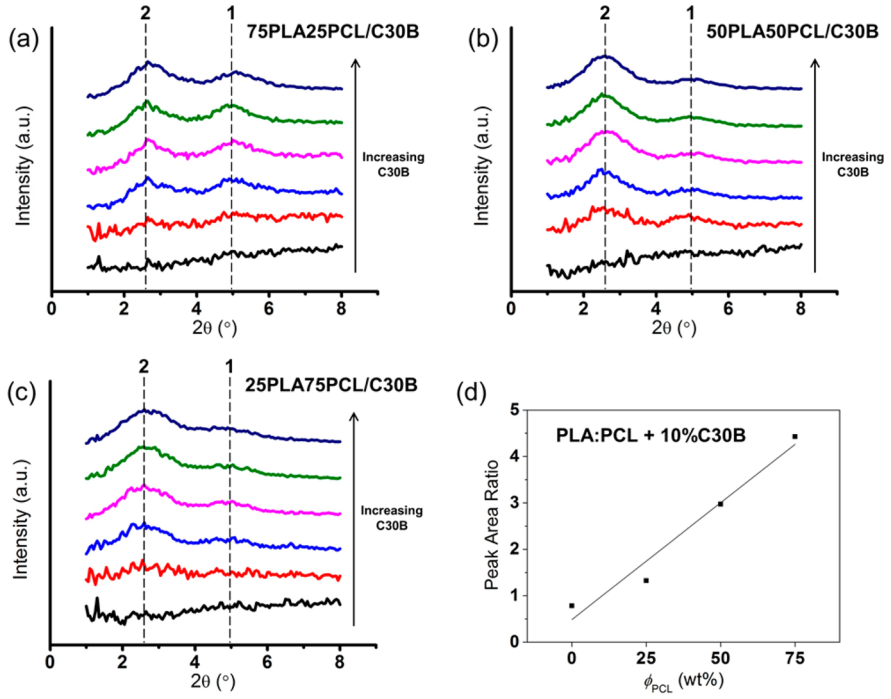

Figure 8. (a) WAXS spectra of 75PLA25PCL/C30B system; (b) WAXS spectra of 50PLA50PCL/C30B system; (c) WAXS spectra of 25PLA75PCL/C30B system; and (d) area ratios between peaks 2 and 1 in PLA:PCL +10 wt % C30B as a function of PCL concentration.

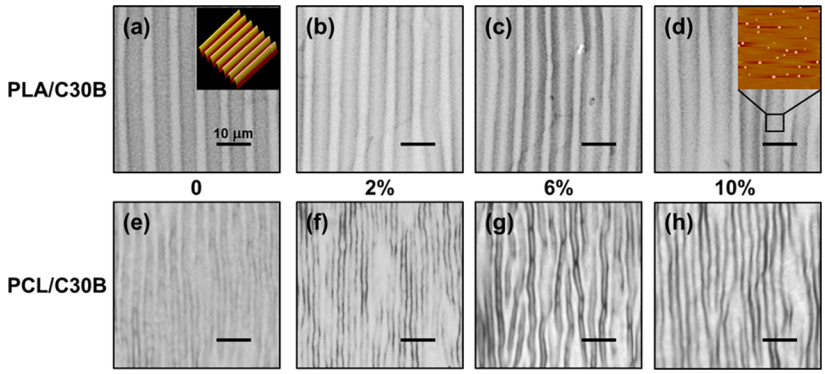

Figure 9. Optical micrographs of thin films after buckling: (a) neat PLA, inset showing AFM height image of buckling patterns (scan size 50 μm); (b) PLA + 2% C30B; (c) PLA + 6% C30B; (d) PLA + 10% C30B, inset showing AFM phase image of C30B in PLA (scan size 5 μm); (e) neat PCL; (f) PCL + 2% C30B; (g) PCL + 6% C30B; and (h) PCL + 10% C30B. Scale bars of optical micrographs represent 10 μm.

modulus of thin films after buckling.[32] However, the amplitude is dependent on the elastic strain, which introduces another parameter and complicates the analysis. In this study only the buckling wavelength is used for elastic modulus calculation.

Buckling patterns are also observed by optical microscopy for nanocomposite thin films. Comparing nanocomposite thin films (Figure 9b–d and f–h) with homopolymer thin films (Figure 9a,e), it is obvious that adding C30B in the films introduces in-plane inhomogeneity to the buckling patterns. The reason is that C30B formed small aggregates in the films, which have a much higher modulus compared with polymers and prevented it from bending. As a result, the buckles have to travel around C30B aggregates, perturbing the sinusoidal periodicity. Despite that, the overall buckling behavior is not arrested since C30B was generally well dispersed and the aggregates were much smaller than the buckling wavelength. Therefore, the SIEBIMM analysis is applicable to PLA/C30B and PCL/C30B nanocomposite thin films and valid for estimating an average film modulus, which was obtained by averaging the buckling wavelength over large areas, as done by FFT of optical micrographs. The dispersion of C30B in the polymer films was also observed by AFM at a scale finer than the buckling wavelength. The inset of Figure 9d is the AFM phase image of a local region in PLA + 10 wt % C30B showing random distribution of C30B in PLA. The nanoclay platelets were found to be parallel to the substrate, which matches previous results by GIWAXS. Buckling patterns are not seen in this AFM image due to the small scan size (5 μm).

The calculated elastic moduli of neat polymer and nanocomposite thin films are plotted in Figure 10. As seen in panel a, neat PLA has an elastic modulus of 2.08 GPa. Adding only 2 wt % C30B significantly increases the modulus by 26% to 2.63 GPa. However, adding more C30B does not further enhance the material. The elastic modulus of PLA/C30B nanocomposite thin films remains generally stable at around 2.50 GPa from 2 to 10 wt % C30B.

In the case of the PCL system (Figure 10b), a much lower elastic modulus of 228 MPa is found for neat PCL. This is

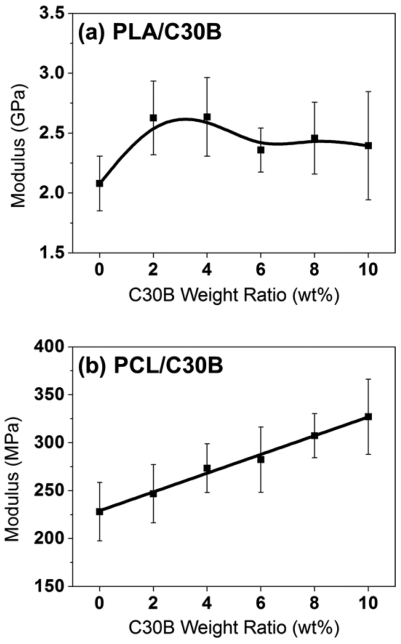

Figure 10. Elastic moduli of nanocomposite thin films as a function of C30B weight ratio in (a) PLA/C30B system and (b) PCL/C30B system.

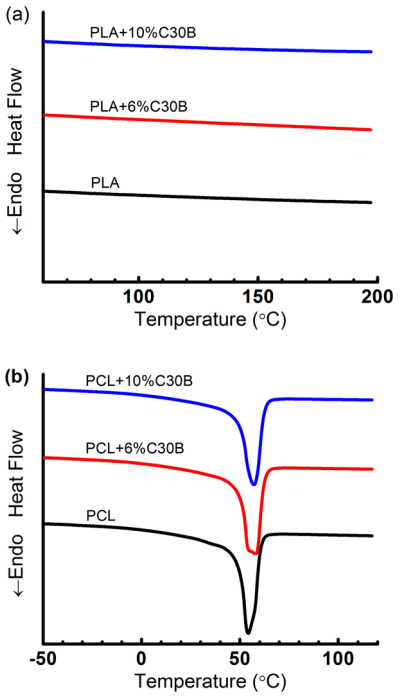

Figure 11. DSC curves of (a) PLA/C30B and (b) PCL/C30B systems.

expected since the glass transition temperature (T_g) of PCL is about −60 °C, whereas that of PLA is around +60 °C. Similar to the PLA system, the strengthening effect of C30B is observed with only 2 wt % C30B addition. However, the two systems behave distinctly differently at higher concentrations of C30B. Modulus of PCL/C30B nanocomposite thin films increases almost linearly from 248 MPa for 2 wt % C30B to 327 MPa for 10 wt % C30B. The coefficient of determination R^2 is 0.987 indicating excellent linearity. The slope, $\Delta E/\Delta c$, is found to be 9.78 MPa/wt % C30B.

For semicrystalline polymers, it is well-known that the elastic modulus is closely related to the crystallinity, which could be affected by the presence of nanoparticles. As a result, the study on elastic modulus needs to be accompanied by measurements of crystallinity in order to clarify the strengthening mechanism. In this study, instead of semicrystalline poly(L-lactide) (PLLA) or poly(D-lactide) (PDLA), we used amorphous poly(D,L-lactide) polymerized from a racemic mixture of L- and D-lactides. Note this is different from blends of PLLA and PDLA, which were reported to have unique crystalline structures.[33,34] On the other hand, PCL is a semicrystalline polymer. The crystallinity of both nanocomposite systems was studied by DSC as shown in Figure 11. No melting peak was observed in PLA/C30B system (Figure 11a), indicating completely amorphous state regardless of the amount of C30B. In contrast, each curve shows a melting peak suggesting semicrystalline state in PCL/C30B system (Figure 11b). The enthalpy of fusion was measured by software and corrected by the weight ratio of PCL. The percentage of crystallinity were calculated by dividing the enthalpy of fusion for 100% crystalline PCL (139.5 J/g[35]). Results of PCL/C30B system are listed in Table 1, showing a consistent crystallinity around 50%, which is independent of the weight ratio of C30B. Therefore, adding C30B does not change the original crystallinity of either PLA or PCL, hence there should be no impact on the elastic modulus from the crystallinity aspect. There is a small increase in crystal melting temperature (T_m) that can be attributed to an entropic effect of adding clay given that there is no enthalpic effect from the endotherms. We conclude that the strengthening behavior in PLA/C30B and PCL/C30B systems observed by SIEBIMM is solely the result of polymer/nanoparticle interaction.

Table 1. Enthalpy of Fusion and Crystallinity of PCL/C30B System

	enthalpy of fusion (J/g)	crystallinity (%)
PCL	67.21	48.2
PCL + 6% C30B	71.21	51.0
PCL + 10% C30B	69.96	50.1

DISCUSSIONS

As mentioned earlier, the dispersion states and strengthening effects of nanoclays, including C30B, have been previously explored thoroughly in both biopolymers, PLA- and PCL-based nanocomposites in their bulk forms.[19−24] However, to the best of our knowledge, this is the first time that submicron thin films of PLA/C30B and PCL/C30B are investigated using high throughput techniques. We conclude that the strengthening effect of nanocomposite thin films is directly related to the interaction controlled dispersion of C30B in the polymer matrix. C30B was partially intercalated by PLA and strengthening effect was observed for up to 2 wt % addition. Thereafter, adding more C30B provided no further enhancement. C30B was almost completely intercalated by PCL and well dispersed with up to 10 wt % addition, thus giving a continuous and linear strengthening effect.

A possible explanation to the difference in strengthening effects of C30B in PLA and in PCL is proposed here from the molecular structure perspective. While both polymers have hydrogen bonding capability with C30B, PLA has short side groups, making the polymer chain difficult to align. In contrast, PCL has a linear and flexible chain. When layered C30B is added to the polymer matrix, it is easier for PCL molecules to

diffuse in-between C30B layers and expand the interlayer distance. Therefore, PCL has a better chance to form intercalated or even exfoliated structure with C30B nanoparticles, thus giving rise to the difference in the strengthening behavior. Homogeneous blend systems of PLA:PCL/C30B nicely confirm the interpolative nature of the dispersion based behavior with WAXS results.

We would like to emphasize the issue that the state of dispersion of nanoparticles in thin films can be different from that in bulk materials. Ozkoc and Kemaloglu reported mostly intercalated or partially exfoliated structures in PLA/C30B nanocomposites, and the dispersion state was further improved to complete exfoliation with PEG plasticizer.[19] Istrate and Chen found coexistence of intercalated and exfoliated structures in PCL/C30B systems.[24] The underlying reason for such differences pertains to the processing method. Melt blending was utilized in those cases for bulk nanocomposites, while solution mixing was used in our study to make thin films. Among the common processing methods of nanocomposites, melt blending is usually favored, as it allows diffusion and interaction of polymer chains and nanoclay platelets by shearing at elevated temperatures.[36,37] Polymer molecules thus have enough mobility and time to migrate into the galleries of nanoclays and separate the layers, leading to intercalated or exfoliated structures. In contrast, solution mixing does not guarantee uniform dispersion of nanoclays in polymers, which requires the correct combination of polymer, nanoparticle, and solvent.[38] As seen in this study, intercalated structures were formed in PCL/C30B/toluene system, while PLA/C30B/toluene system was only partially intercalated. In spite of the limited mixing power, solution mixing is the only known feasible method to prepare submicron nanocomposite thin films. More importantly, it is capable of making gradient high throughput samples with the help of the flow-coating technique, which greatly improves efficiency and opens routes for a variety of applications.

Despite the difference in processing method, our modulus measurements on PCL/nanoclay thin films by SIEBIMM are found to match with bulk values reported earlier. Using a similar nanoparticle, MMT, Lepoittevin et al. reported an increased modulus from 217 MPa for neat PCL to 365 MPa for PCL + 10% MMT,[21] which is in good agreement with our results of 228 MPa for neat PCL and 327 MPa for PCL +10% C30B. The agreement is expected because C30B was well dispersed and almost completely intercalated in PCL thin films by solution mixing, not significantly different from the dispersion state of C30B in bulk PCL by melt blending. The comparison indicates that even at the submicron scale (70−150 nm), the moduli of homopolymer and nanocomposite thin films retain their bulk values. This is also within expectation since researchers found dramatically decreased modulus of thin films only at much smaller thicknesses (<40 nm).[39] Further investigation on the effect of nanoparticles on moduli of ultrathin films is in progress.

When studying the elastic modulus of polymer nanocomposites, composite theories help to establish a descriptive model and predict the modulus from properties of the components. The Halpin−Tsai model was found to be very useful in polymer nanocomposites with oriented nanoparticles.[40] It is worth mentioning that the Halpin−Tsai model is only applicable to uniformly distributed nanocomposites, which is not the case for many clay-biopolymer nanocomposite systems. Researchers have proposed several modifications to the Halpin−Tsai model for clay−polymer nanocomposites.[41−43] However, each modification introduces extra parameters and their applications remain limited. In this study, we used the original Halpin−Tsai model and applied it to the PCL/C30B system, since the dispersion of C30B in PCL is fairly uniform. Due to the intercalation behavior of C30B in PCL, several intercalated C30B layers and the polymer molecules form one "effective nanoparticle". It is therefore difficult to define an aspect ratio of nanoparticles. Instead, we used it as a parameter and fit the experimental data of elastic moduli of PCL/C30B as shown in Figure 12.

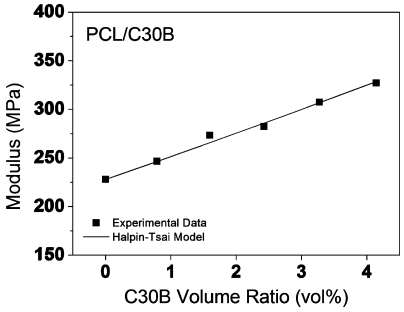

Figure 12. Fitting of elastic moduli of the PCL/C30B system using the Halpin−Tsai model.

The best fit of this parametric "aspect ratio" (l/d) was found to be 4.68. In comparison, the theoretical aspect ratio for individual C30B layers is about 110 (Southern Clay Products). The large difference is reasonable since intercalation was observed in PCL/C30B rather than exfoliation. A previous study obtained an effective aspect ratio of 7.53 in the same system prepared in bulk by melt blending,[44] 61% larger than in the present study, which again demonstrates the limited mixing power of solution mixing compared with melt blending.

CONCLUSIONS

PLA/C30B and PCL/C30B nanocomposite thin films were prepared and their structures and elastic moduli were characterized. As shown by WAXS, GIWAXS, and TEM results, C30B nanoclays are moderately dispersed in PLA but well dispersed and almost completely intercalated in PCL. In addition, the dispersion of C30B improves continuously with increasing PCL content in blends of PLA:PCL. Strengthening effect of C30B was observed in both PLA and PCL systems with only 2 wt % addition. At higher loadings of C30B, elastic modulus of PLA/C30B nanocomposite remained stable, while that of the PCL/C30B nanocomposite increased continuously. Enrichment of the organoclay was observed at the film surface as confirmed by XPS and their surface water contact angle was reflective of this film morphology. Further, the organoclays were oriented parallel to the film surface, a morphology useful for barrier film applications. Controlled clay dispersion and orientation have notable significance, from gas and liquid permeation barrier films to enhancing film dielectric properties to UV blocking layers for solar cells, potentially enabling use of these clay−biopolymer nanocomposite thin films for energy and sustainable technologies.

AUTHOR INFORMATION

Corresponding Author

*E-mail: alamgir@uakron.edu.

Present Addresses

[‖]Gurpreet Singh, Intel Corporation, 2501 NW 229th Ave, Hillsboro, OR 97124, United States.

[⊥]Ahmed Elzatahry, Polymer Materials Research Department, Advanced Technology and New Materials Research Institute, City of Scientific Research and Technology Applications, New Borg El-Arab City Alexandria 21934, Egypt.

Notes

The authors declare no competing financial interest.

■ ACKNOWLEDGMENTS

This work was supported by AFOSR Grant FA9550-12-1-0306 and the Akron Functional Materials Center (AFMC). Acknowledgment is made to the donors of the American Chemical Society Petroleum Research Fund for support of this research. The GIWAXS work was supported by DOE Grant DE-FG02-10ER4779. We thank Prof. Bryan Vogt and Changhuai Ye for help with the PDMS strain stage and Dr. Bojie Wang for TEM imaging. H.Y. would like to thank Ryan Schmidt, Dr. Manish Kulkarni, and Dr. Jolanta Marszalek-Kempke for fruitful discussion and Danielle Grolman for review of the manuscript. Analysis of the homogeneity and dispersion of the nano filler clay within the polymer films for suitability for dielectrics and future glass transition studies was enabled by support from the W.M. Keck Foundation.

■ REFERENCES

(1) Chen, G.-Q.; Patel, M. K. Plastics Derived from Biological Sources: Present and Future: A Technical and Environmental Review. *Chem. Rev.* **2012**, *112*, 2082−2099.

(2) Khare, A.; Deshmukh, S. Studies Toward Producing Eco-Friendly Plastics. *J. Plast. Film Sheeting* **2006**, *22*, 193−211.

(3) Van de Velde, K.; Kiekens, P. Biopolymers: Overview of Several Properties and Consequences on Their Applications. *Polym. Test.* **2002**, *21*, 433−442.

(4) Lunt, J. Large-Scale Production, Properties and Commercial Applications of Polylactic Acid Polymers. *Polym. Degrad. Stab.* **1998**, *59*, 145−152.

(5) Darder, M.; Aranda, P.; Ruiz-Hitzky, E. Bionanocomposites: A New Concept of Ecological, Bioinspired, and Functional Hybrid Materials. *Adv. Mater.* **2007**, *19*, 1309−1319.

(6) Avella, M.; De Vlieger, J. J.; Errico, M. E.; Fischer, S.; Vacca, P.; Volpe, M. G. Biodegradable Starch/clay Nanocomposite Films for Food Packaging Applications. *Food Chem.* **2005**, *93*, 467−474.

(7) Sinha Ray, S.; Okamoto, M. Polymer/layered Silicate Nanocomposites: A Review from Preparation to Processing. *Prog. Polym. Sci.* **2003**, *28*, 1539−1641.

(8) Masser, K. A.; Yuan, H.; Karim, A.; Snyder, C. R. Polymer Chain Dynamics in Intercalated Poly(ε-caprolactone)/Nanoplatelet Blends. *Macromolecules* **2013**, *46*, 2235−2240.

(9) Mittal, V. In *Biopolymer Nanocomposites: Processing, Properties, and Applications*; Dufresne, A., Thomas, S., Pothen, L. A., Eds.; John Wiley & Sons, Inc.: Hoboken, NJ, 2013; pp 541−563.

(10) Rowe, B. W.; Freeman, B. D.; Paul, D. R. Physical Aging of Ultrathin Glassy Polymer Films Tracked by Gas Permeability. *Polymer (Guildf)* **2009**, *50*, 5565−5575.

(11) Stafford, C. M.; Harrison, C.; Beers, K. L.; Karim, A.; Amis, E. J.; VanLandingham, M. R.; Kim, H.-C.; Volksen, W.; Miller, R. D.; Simonyi, E. E. A Buckling-Based Metrology for Measuring the Elastic Moduli of Polymeric Thin Films. *Nat. Mater.* **2004**, *3*, 545−550.

(12) Volynskii, A. L.; Bazhenov, S.; Lebedeva, O. V.; Bakeev, N. F. Mechanical Buckling Instability of Thin Coatings Deposited on Soft Polymer Substrates. *J. Mater. Sci.* **2000**, *35*, 547−554.

(13) Nolte, A. J.; Rubner, M. F.; Cohen, R. E. Determining the Young's Modulus of Polyelectrolyte Multilayer Films via Stress-Induced Mechanical Buckling Instabilities. *Macromolecules* **2005**, *38*, 5367−5370.

(14) Kim, Y. H.; Lee, Y. M.; Lee, J. Y.; Ko, M. J.; Yoo, P. J. Hierarchical Nanoflake Surface Driven by Spontaneous Wrinkling of Polyelectrolyte/metal Complexed Films. *ACS Nano* **2012**, *6*, 1082−1093.

(15) Huang, H.; Chung, J. Y.; Nolte, A. J.; Stafford, C. M. Characterizing Polymer Brushes via Surface Wrinkling. *Chem. Mater.* **2007**, *19*, 6555−6560.

(16) Wilder, E. A.; Guo, S.; Lin-Gibson, S.; Fasolka, M. J.; Stafford, C. M. Measuring the Modulus of Soft Polymer Networks via a Buckling-Based Metrology. *Macromolecules* **2006**, *39*, 4138−4143.

(17) Ye, C.; Singh, G.; Wadley, M.; Karim, A. Anisotropic Mechanical Properties of Aligned Polystyrene-Block-Polydimethylsiloxane Thin Films. *Macromolecules* **2013**, *46*, 8608−8615.

(18) Lee, J.-Y.; Su, K. E.; Chan, E. P.; Zhang, Q.; Emrick, T.; Crosby, A. J. Impact of Surface-Modified Nanoparticles on Glass Transition Temperature and Elastic Modulus of Polymer Thin Films. *Macromolecules* **2007**, *40*, 7755−7757.

(19) Ozkoc, G.; Kemaloglu, S. Morphology, Biodegradability, Mechanical, and Thermal Properties of Nanocomposite Films Based on PLA and Plasticized PLA. *J. Appl. Polym. Sci.* **2009**, *114*, 2481−2487.

(20) Zaidi, L.; Bruzaud, S.; Bourmaud, A.; Mederic, P.; Kaci, M.; Grohens, Y. Relationship between Structure and Rheological, Mechanical and Thermal Properties of polylactide/Cloisite 30B Nanocomposites. *J. Appl. Polym. Sci.* **2009**, *116*, 1357−1365.

(21) Lepoittevin, B.; Pantoustier, N.; Devalckenaere, M.; Alexandre, M.; Calberg, C.; Jérôme, R.; Henrist, C.; Rulmont, A.; Dubois, P. Polymer/layered Silicate Nanocomposites by Combined Intercalative Polymerization and Melt Intercalation: A Masterbatch Process. *Polymer (Guildf)* **2003**, *44*, 2033−2040.

(22) Di, Y.; Iannace, S.; Di Maio, E.; Nicolais, L. Nanocomposites by Melt Intercalation Based on Polycaprolactone and Organoclay. *J. Polym. Sci., Part B: Polym. Phys.* **2003**, *41*, 670−678.

(23) Pluta, M.; Paul, M.-A.; Alexandre, M.; Dubois, P. Plasticized Polylactide/clay Nanocomposites. II. The Effect of Aging on Structure and Properties in Relation to the Filler Content and the Nature of Its Organo-Modification. *J. Polym. Sci., Part B: Polym. Phys.* **2006**, *44*, 312−325.

(24) Istrate, O. M.; Chen, B. Porous Exfoliated Poly(ε-Caprolactone)/clay Nanocomposites: Preparation, Structure, and Properties. *J. Appl. Polym. Sci.* **2012**, *125*, E102−E112.

(25) Stafford, C. M.; Roskov, K. E.; Epps, T. H.; Fasolka, M. J. Generating Thickness Gradients of Thin Polymer Films via Flow Coating. *Rev. Sci. Instrum.* **2006**, *77*, 023908.

(26) Stafford, C. M.; Guo, S.; Harrison, C.; Chiang, M. Y. M. Combinatorial and High-Throughput Measurements of the Modulus of Thin Polymer Films. *Rev. Sci. Instrum.* **2005**, *76*, 062207.

(27) Roth, S. V.; Burghammer, M.; Riekel, C.; Müller-Buschbaum, P.; Diethert, A.; Panagiotou, P.; Walter, H. Self-Assembled Gradient Nanoparticle-Polymer Multilayers Investigated by an Advanced Characterization Method: Microbeam Grazing Incidence X-Ray Scattering. *Appl. Phys. Lett.* **2003**, *82*, 1935.

(28) Müller-Buschbaum, P.; Roth, S. V.; Burghammer, M.; Diethert, A.; Panagiotou, P.; Riekel, C. Multiple-Scaled Polymer Surfaces Investigated with Micro-Focus Grazing-Incidence Small-Angle X-Ray Scattering. *Europhys. Lett.* **2003**, *61*, 639−645.

(29) Müller-Buschbaum, P.; Perlich, J.; Abul Kashem, M. M.; Schulz, L.; Roth, S. V.; Cheng, Y. J.; Gutmann, J. S. Combinatorial Investigation of Nanostructures Formed in a Titanium Dioxide Based Nanocomposite Film on Top of Fluor-Doped Tin Oxide Layers. *Phys. Status Solidi − Rapid Res. Lett.* **2007**, *1*, 119−121.

(30) Perlich, J.; Rubeck, J.; Botta, S.; Gehrke, R.; Roth, S. V.; Ruderer, M. A.; Prams, S. M.; Rawolle, M.; Zhong, Q.; Körstgens, V.; Müller-Buschbaum, P. Grazing Incidence Wide Angle X-Ray Scattering at the Wiggler Beamline BW4 of HASYLAB. *Rev. Sci. Instrum.* **2010**, *81*, 105105.

(31) Han, C. On the Mechanisms Leading to Exfoliated Nanocomposites Prepared by Mixing. *Adv. Polym. Sci.* **2010**, *231*, 1−75.
(32) Huang, R. Kinetic Wrinkling of an Elastic Film on a Viscoelastic Substrate. *J. Mech. Phys. Solids* **2005**, *53*, 63−89.
(33) Ikada, Y.; Jamshidi, K.; Tsuji, H.; Hyon, S. H. Stereocomplex Formation between Enantiomeric Poly(lactides). *Macromolecules* **1987**, *20*, 904−906.
(34) Urayama, H.; Kanamori, T.; Fukushima, K.; Kimura, Y. Controlled Crystal Nucleation in the Melt-Crystallization of Poly(l-Lactide) and Poly(l-Lactide)/poly(d-Lactide) Stereocomplex. *Polymer (Guildf)* **2003**, *44*, 5635−5641.
(35) Wang, Y.; Rodriguez-Perez, M. A.; Reis, R. L.; Mano, J. F. Thermal and Thermomechanical Behaviour of Polycaprolactone and Starch/Polycaprolactone Blends for Biomedical Applications. *Macromol. Mater. Eng.* **2005**, *290*, 792−801.
(36) Pavlidou, S.; Papaspyrides, C. D. A Review on Polymer−layered Silicate Nanocomposites. *Prog. Polym. Sci.* **2008**, *33*, 1119−1198.
(37) Alexandre, M.; Dubois, P. Polymer-Layered Silicate Nanocomposites: Preparation, Properties and Uses of a New Class of Materials. *Mater. Sci. Eng. R-Rep.* **2000**, *28*, 1−63.
(38) Ogata, N.; Jimenez, G.; Kawai, H.; Ogihara, T. Structure and Thermal/mechanical Properties of Poly(l-Lactide)-Clay Blend. *J. Polym. Sci., Part B: Polym. Phys.* **1997**, *35*, 389−396.
(39) Stafford, C. M.; Vogt, B. D.; Harrison, C.; Julthongpiput, D.; Huang, R. Elastic Moduli of Ultrathin Amorphous Polymer Films. *Macromolecules* **2006**, *39*, 5095−5099.
(40) Halpin, J.; Kardos, J. The Halpin-Tsai Equations: A Review. *Polym. Eng. Sci.* **1976**, *16*, 344−352.
(41) Yung, K. C. Modeling Young's Modulus of Polymer-Layered Silicate Nanocomposites Using a Modified Halpin–Tsai Micromechanical Model. *J. Reinf. Plast. Compos.* **2006**, *25*, 847−861.
(42) Mohapatra, A. K.; Mohanty, S.; Nayak, S. K. Modeling of the Mechanical Properties of Polylactic Acid/clay Nanocomposites Using Composite Theories. *Int. J. Plast. Technol.* **2012**, *15*, 174−187.
(43) Wu, Y.-P.; Jia, Q.-X.; Yu, D.-S.; Zhang, L.-Q. Modeling Young's Modulus of Rubber−clay Nanocomposites Using Composite Theories. *Polym. Test.* **2004**, *23*, 903−909.
(44) Pérez, C. J.; Alvarez, V. A.; Mondragón, I.; Vázquez, A. Mechanical Properties of Layered Silicate/starch Polycaprolactone Blend Nanocomposites. *Polym. Int.* **2007**, *56*, 686−693.